Precessing magnetic particles as ac magnetic field sensors

A. T. M. Anishur Rahman*

Electromagnetic waves are widely used including in defense, biomedicine, and fundamental science. Their efficient detection determines how we communicate, defend against adversaries, diagnose diseases and perform search and rescue operations. In this article, exploiting the precession of a levitated magnetic particle in ultra-high vacuum, we show that weak electromagnetic waves down to the femtotesla level can be detected. It is also shown that such a sensor has a large dynamic range over a millitesla, is continuously tunable over many gigahertz and can detect frequencies with sub-hertz resolutions. The direction of arrival of the incoming electromagnetic wave can also be found relatively easily.

The ability to detect electromagnetic (EM) fields has applications, among others, in fundamental physics [1–4], radar [5], biomedicine [6–8], search and rescue [9], climate monitoring [10] and wireless communications [11]. In fundamental physics, microwave sensors have been used for the detection of cosmic microwave background [1] and fast radio bursts [2] and suggested for the search for dark matter [3, 4, 12]. In biomedicine, EM sensors are used for monitoring various aspects of our health including cardiopulmonary activities [6, 7] and breast cancer [8] whilst in search and rescue operations such sensors are deployed to detect living things hidden beneath rubble [9]. Likewise, the detection of civil and military aircraft is routinely performed using EM sensors [5].

Traditionally, EM waves are detected using antennas which, once made, cannot be changed and have a limited frequency range of operation. In principle, EM fields can be detected using either an electric or a magnetic field sensor. Examples of electric field sensors include Rydberg atoms [13–15]. In Autler-Townes configuration such a sensor can detect discrete frequencies between MHz and THz [13, 16] and fields as weak as $\approx 5~\mu$V/m (1.7×10^{-14} T) [13, 14, 17]. Existing magnetic field sensors such as atomic vapors [18] and the nitrogen-vacancy centre (NVC) in diamond-based sensors [19] are predominantly used as dc field sensors, although some progress has been made towards the detection of EM fields using NVCs in diamond [20]. Such magnetic field sensors have a relatively small dynamic range e.g., $\leq \mu$T. Superconducting quantum interference devices are excellent magnetic field sensors but require cryogenic temperatures [21]. Efficient sensing of EM waves can enhance our capability to defend against adversaries by detecting the weakest possible signals and hence providing early warnings [5], perform better search and rescue operations by detecting faint signals from living things hidden under rubble [9], and diagnose diseases [6–8]. Re-configurable detectors, in particular detectors which can be configured for different frequencies on demand while in operation, would also benefit the aforementioned areas.

Levitation in vacuum provides a contactless and a near-frictionless environment. This makes levitated particles susceptible to external stimuli making them ex-

tremely good sensors. For example, using the center-of-mass motions of such particles, zeptonewton scale force sensitivity has been achieved [22]. Likewise, exploiting the rotational motion of a levitated particle, extremely small torque has been measured [23]. Among levitated particles, magnetic particles are unique in the sense that they contain an extra degree of freedom i.e., the spin which makes them even more versatile. The coupling between the spin and the other degrees of freedom of a levitated magnetic particle has not been explored yet but is promising for developing new technologies [24] and exploring fundamental physics [25].

In this article, using the precessional motion of a levitated magnetic particle in ultra-high vacuum, it is shown that extremely weak electromagnetic waves of femtotesla (10^{-15} T) strength can be detected. Such a magnetometer has a dynamic range over a millitesla, can be continuously tuned over many GHz and detect frequencies with sub-hertz resolutions. It is also shown that the direction of arrival of the EM wave can be determined relatively easily.

Consider a magnetic sphere of moment $\boldsymbol{\mu}$ polarized along its easy magnetization axis levitated inside a vacuum chamber. A homogeneous dc magnetic field B_a (Fig. 1) is applied along the $+z$ axis which ensures $\boldsymbol{\mu}$ aligns with B_a i.e., $\boldsymbol{\mu} = [0~0~\mu_s]$, where μ_s is the saturated magnetic moment of the levitated particle. Consider also that an electromagnetic plane wave whose frequency ω and strength $\mathbf{b}$ we aim to determine is propagating in the $+z$ direction and illuminates the magnetic particle. The interaction between the EM wave and the spins or magnetization initiates a spin precession in the ferromagnetic particle [26, 27] giving rise to components of magnetic moment in the xy plane. The dynamics of spin precession can be modeled using the Landau-Lifshitz-Gilbert equation [27]

$$\frac{d\boldsymbol{\mu}}{dt} = \gamma \boldsymbol{\mu} \times \mathbf{B} - \frac{\alpha}{\mu_s}(\boldsymbol{\mu} \times \frac{d\boldsymbol{\mu}}{dt}), \qquad (1)$$

where $\mathbf{B} = b_0 \cos \omega t~\hat{x} + \sigma b_0 \sin \omega t~\hat{y} + B_0~\hat{z}$, γ is the gyromagnetic ratio, $B_0 = B_a + B_{an}$ with B_{an} being the effective field associated with the magnetocrystalline anisotropy [28], and $\alpha > 0$ is the dimensionless Gilbert
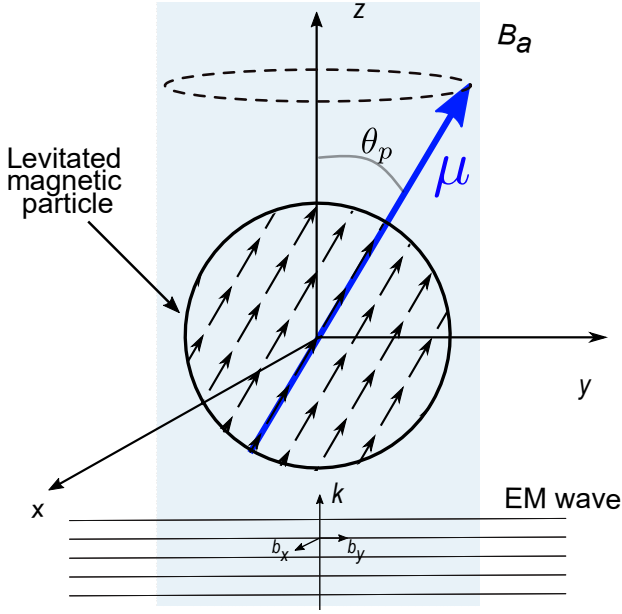
FIG. 1. Precession of a levitated magnet when exposed to electromagnetic waves. The light blue background represents a homogeneous dc magnetic field B_a. A circularly polarized electromagnetic (EM) wave propagating along the z axis initiates spin precession which subsequently induces a mechanical precession. The mechanical angle of precession is denoted by θ_p. The wavevector of the electromagnetic wave is represented by $\mathbf{k}$. The magnetic field associated with the EM wave is in the $x-y$ plane with $b_x = b_0 \cos \omega t$, $b_y = \sigma b_0 \sin \omega t$ and $\sigma = \pm 1$. When $\sigma = +1$ ($\sigma = -1$) the incoming EM wave rotates anticlockwise (clockwise).

damping constant. $\mathbf{b} = b_0 \cos \omega t \ \hat{x} + \sigma b_0 \sin \omega t \ \hat{y}$ is the magnetic component of the EM field and σ determines its direction of rotation e.g., $\sigma = -1$ (+1) corresponds to clockwise (anticlockwise) rotation. $\mathbf{b}$ is the field that we aim to detect. Equation (1) has no general analytical solution. However, when $b \ll B_0$, one can approximate $\mu_z \approx \mu_s$ and $\frac{d\mu_z}{dt} \approx 0$. Under these conditions [29, 30], the steady state solution of (1) is given by

$$\mu_x = \frac{b_0 \gamma m_s}{\sqrt{(\gamma B_0 + \sigma \omega)^2 + \alpha^2 \omega^2}} \cos(\omega t - \beta), \quad (2)$$

where β is the phase difference between $\mathbf{b}$ and the precession of spins or magnetization and is given by $\beta = \tan^{-1}[\frac{\alpha \omega}{\gamma B_0 + \sigma \omega}]$. A similar expression for μ_y exists except $\cos(\omega t - \beta)$ is replaced by $\sin(\omega t - \beta)$ in (2). Importantly, when $\sigma = -1$, μ_x has a Lorentzian profile and has a full-width half-maximum linewidth of $\approx \sqrt{12\alpha^2\gamma^2 B_0^2}$. μ_x reaches its maximum when $\omega = \gamma B_0$. This is known as the ferromagnetic resonance (FMR). On FMR the amplitude of μ_x is $b_x \mu_s / \alpha B_0$. In contrast, when $\sigma = +1$, the rotating EM field opposes the precession of the magnetization [31] and hence the induced magnetic moment in the $x-y$ plane is several orders of

magnitude smaller compared to the FMR case since, in our case, ω is in gigahertz and for most material [32–35] $0 < \alpha \ll 1$. Note that when $\mathbf{B_a}$ is applied along the $-z$ axis, a counterclockwise rotating ($\sigma = +1$) EM field can excite the FMR [31].

In a ferromagnetic material spins and thus magnetization are connected to the crystal lattice via magnetocrystalline anisotropy [26]. This provides a link between the internal (spin) and the mechanical degrees of freedom of a magnetic object. For a levitated magnet, this connectivity means that when the magnetization starts to precess, the crystal lattice and thus the levitated particle attempt to follow it [24, 29, 36, 37]. Precessions of levitated magnets can be detected using the optical interferometric scheme used in levitated optomechanics [23, 38–41]. For a levitated magnet to precess mechanically, however, it must overcome the resistance that it encounters from the residual gas molecules inside the vacuum chamber. The resistive torque [42] that an object faces at a precession frequency Ω_p is $I\Omega_p\Gamma_g$, where I is the moment of inertia, and Γ_g is the damping rate due to gas molecules. In contrast, the driving torque due to the incoming EM field is given by the right hand side of (1) normalized by γ [26]. At equilibrium when the driving and the resistive torques are equal, the precession frequency is

$$\Omega_p = \frac{1}{I\Gamma_g} \frac{b_0 \mu_s \omega}{\sqrt{(\gamma B_0 + \sigma \omega)^2 + \alpha^2 \omega^2}}, \quad (3)$$

Note that (3) alone cannot uniquely determine the frequency of the unknown EM wave. This is because when the driving torque is less than the resistive torque, the magnet would precess at a lower rate and hence taking the mechanical precession rate as the frequency of the EM wave would be inaccurate. This, however, can be avoided by measuring the precession frequency as a function of the damping rate or the gas pressure P ($\Gamma_g \propto P$). As P decreases, Ω_p increases. But, when Ω_p reaches the frequency of the unknown EM field, Ω_p remains constant as Γ_g decreases. This is a consequence of the driven nature of mechanical motions which prefer to synchronize with the frequency of the driving fields [29, 36] (see (2)). At the critical damping rate Γ_g^c where $\Omega_p = \omega$, the mechanical precession frequency directly determines the frequency of the EM wave while the strength of the unknown EM field is

$$b_0 = \frac{I\Gamma_g^c}{\mu_s} \sqrt{(\gamma B_0 + \sigma \omega)^2 + \alpha^2 \omega^2}. \quad (4)$$

From (4) it is clear that our detector is most sensitive at the ferromagnetic resonance i.e., $\sigma = -1$. The occurrence of FMR can be ensured by checking that the mechanical precession frequency is equal to γB_0. Otherwise, B_a can be adjusted such that it matches the mechanical
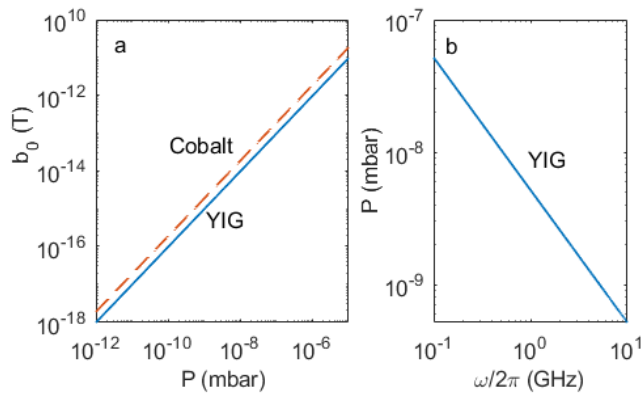
FIG. 2. a) On ferromagnetic resonance the minimum detectable magnetic field as a function of residual gas pressure when the precession frequency or the frequency of the unknown EM wave is 5 GHz with a YIG ($M = 1.4 \times 10^5$ A/m and $\alpha = 5.58 \times 10^{-5}$) or a cobalt ($M = 1.4 \times 10^6$ A/m and $\alpha = 0.01$) sphere ($r = 100$ nm) as a sensor. b) The minimum required gas pressure for sensing EM fields of different frequencies with $b_0 = 10^{-15}$ T when a YIG sphere (100 nm) is used.

precession frequency. Moreover, since on FMR the driving torque is maximum, the mechanical precession at γB_0 is expected to happen at a higher Γ_g^c compared to non-resonant cases. When the FMR condition is satisfied, the minimum detectable field is

$$ b_0 = \frac{2\alpha\omega\Gamma_g^c \rho r^2}{5M}, \tag{5} $$

where we have substituted $I = 2\rho v r^2/5$ and $\mu_s = vM$ with r, ρ, v and M being the radius, the mass density, the volume and the saturation magnetization of the levitated magnet. Parameters such as ρ and M in (5) can be found from the relevant bulk material while α, Γ_g^c and r can be measured experimentally in situ [33, 43, 44].

Let us consider numerical examples for better understanding. Here, any magnetic materials can be used as sensors as long as they can be levitated. Levitation can be carried out using a Paul trap [45–48]. Such a trap uses oscillating electric fields (frequency in KHz) for levitation and can levitate any object as long as they are charged. Due to the small amount of light used in a Paul trap for the detection of levitated particles, resistive torques associated with the radiation pressure and light scattering are negligible [44]. Figure 2a shows the minimum detectable field when a yttrium iron garnet (YIG, a weak magnet) or a cobalt (a strong magnet) sphere ($r = 100$ nm) is used as a sensor. The frequency of the EM field is assumed to be $\omega/2\pi = 5$ GHz and is resonant with the FMR of the levitated magnet. We have also used $\Gamma_g \approx \frac{4P}{\rho v_g}$ with v_g being the velocity of gas molecules [49]. At an experimentally viable pressure of $P = 10^{-9}$ mbar

($\Gamma_g = 2.41 \times 10^{-6}$ rad.), the minimum detectable field is $\approx 2 \times 10^{-15}$ T with cobalt and $\approx 1 \times 10^{-15}$ T with YIG. When converted to electric fields (cb_0), these are equivalent to 6×10^{-7} V/m and 3×10^{-7} V/m, respectively, where c is the speed of light. It is evident that despite cobalt being a strong magnet, YIG is preferable. This is because YIG has a significantly lower Gilbert damping constant [32, 33] compared to cobalt [34] resulting in a lower α/M ratio which provides better sensitivities. At a higher vacuum, which is within experimental reach, even better sensitivities seem feasible (Fig. 2a). Assuming that the target sensitivity is 10^{-15} T, Fig. 2b shows the minimum required residual gas pressure for detecting EM waves of different frequencies when a YIG sphere is used as a sensor. Evidently, EM fields of lower frequencies can be detected at higher gas damping. This is because, at a lower precession frequency, the resistive torque is lower ($\propto \Omega_p$). From (5) it is evident that smaller levitated magnets are better sensors since such objects have significantly lower moments of inertia ($\propto r^5$) requiring smaller driving torques for initiating precessions.

The ability to tune frequencies continuously over a large frequency band is an essential attribute of a versatile EM sensor. In our case, this can be achieved by adjusting B_a, see (2). B_a can be delivered using an electromagnet whose strength can be continuously adjusted by changing the current passing through such a magnet. As B_a changes, the frequency of the ferromagnetic resonance changes allowing the detection of unknown frequencies in a continuous manner. The highest frequency that our sensor can detect is limited by the maximum tensile stress ($\approx \rho\Omega_p^2 r_p^2$), arising from the mechanical precession, that a levitated magnet can withstand [50, 51], where r_p depends on θ_p. Mechanical rotations over 5 GHz have been demonstrated [23] and tens of GHz have been predicted [51]. The lowest frequency that a precessing magnetometer can sense is determined by the saturation magnetization and/or the magnetocrystalline anisotropy of a levitated magnet. In this context, weak magnets such as YIG are preferable since their saturation magnetizations are low. Using levitated YIG spheres as sensors, frequencies down to 200 MHz can be detected [28, 52]. Another key aspect of our sensor is that it can be switched off when required [13], important in defense applications, by turning off the dc bias field. This is in contrast with the classical antennas.

The selectivity of a magnetometer is defined as its ability to detect signals around a given center frequency. It is also known as the Q-factor of a sensor [13]. At a given B_a, our magnetometer is sensitive to frequencies within the ferromagnetic resonance linewidth $\approx \sqrt{12\alpha^2\gamma^2 B_0^2}$ which is dictated by the Gilbert damping constant. For a high selectivity, materials with low α's are required. Here, YIG is an excellent candidate which is known for its extremely narrow FMR linewidth [32, 33, 53]. Using YIG spheres as sensors frequency selectivity of less than a

MHz can be achieved. Importantly, within this frequency band, our magnetometer can resolve frequencies with a sub-hertz resolution. This is a result of it being possible to measure mechanical precession frequencies with high accuracies. For example, rotation frequencies of driven levitated objects have been measured with a resolution better than a mHz [48, 54].

One of the key attributes of a versatile sensor is its ability to remain sensitive when the amplitudes of signals vary widely. This is known as the dynamic range of a sensor. In our case, the angle of precession (Fig. 1) of the levitated magnet and its ability to precess at a given Γ_g are determined by the strength of the unknown oscillating magnetic field. Assuming the magnet is already precessing at ω, as the strength of the EM field increases, the angle of precession of the magnet increases as well. This remains true as long as the strength of the unknown magnetic field is $\ll B_a$. If the unknown field becomes comparable to B_a, the approximation made in deriving (2) e.g., $b_0 \ll B_a$ breaks down. Importantly, as the precession angle increases with the increasing b_0, the detection of precession becomes easier implying an enhanced sensitivity. This is in contrast with other magnetometers which become less sensitive as the strength of the field increases [19, 21]. Generally, B_a is in tens of millitesla implying a large dynamic range e.g., femtotesla to millitesla for a levitated magnet-based magnetometer.

The direction of arrival (DA) of an EM wave is important in many areas of engineering and physics including in defense [55, 56] and astrophysics [2]. In our case, the direction of arrival $\mathbf{k}$ can be found from the direction of $\mathbf{B_a}$. In deriving (4) we assumed that $\mathbf{b}$ is in the $x - y$ plane and hence, in this simple case, the direction of arrival is along the z axis. To further differentiate between the arrival along the $-z$ and the $+z$ directions, the sensor, due to its small size (equivalent to a small vacuum chamber [57]), can be temporarily blocked using an EM absorber [58] from one of the two sides. In the event the EM arrives from the blocked side, the levitated magnet will stop precessing thus determining the arrival direction. For an arbitrary arrival, the direction of $\mathbf{B_a}$ can be adjusted such that $\mathbf{b}$ becomes perpendicular to $\mathbf{B_0}$. This can be ensured by checking that the maximum precession frequency ($\Omega_p = \omega$, see above) is achieved at the highest possible Γ_g^c. This is because when $\mathbf{k}$ is not parallel to $\mathbf{B_a}$, the magnetic component of the EM wave is not orthogonal to $\mathbf{B_a}$. As a result, the torque exerted by $\mathbf{b}$ is not maximal (see Eq. (3)) requiring a reduced Γ_g^c for the magnet to precess at ω. In the extreme case, when $\mathbf{k} \perp \mathbf{B_a}$, there is no torque and the magnet cannot precess.

Finally, let us consider potential sources of noise that can degrade the performance of our sensor. One such source is the fluctuation in the strength of the dc magnetic field B_a. Such fluctuations would change the FMR frequencies and thus the driving torque (see Eq. (4) and the discussion surrounding it). In turn, this can cause uncertainties in the minimum detectable fields. However, highly stable, better than a part-per-billion fluctuation, electromagnets are available [59, 60]. As a result, our sensor is robust.

In conclusion, we have theoretically shown that a levitated magnet in high vacuum is capable of detecting electromagnetic fields with femtotesla sensitivity. When converted to an electric field, this is equivalent to 3×10^{-7} V/m. If achieved experimentally, this would be significantly better than the performance of existing sensors [13–15] with the added benefit of the simplicity of our proposed experiment. The overall sensor size including a vacuum chamber [57] and a Paul trap [48] can be < 1 cm^3. We have also shown that the new magnetometer can be continuously tuned between hundreds of MHz and tens of GHz and remains sensitive when the field strength varies between femtotesla to millitesla. Within the frequency range of operation, the new magnetometer can measure frequencies with a resolution better than a mHz and a selectivity of about a MHz. We envisage that due to its high sensitivity and the ability to be configured for sensing different frequencies by merely changing the externally applied magnetic field, the new magnetometer can be useful in fields such as biomedicine [6, 7], search and rescue [9] and defense [9] where the ability to sense at different frequencies is crucial.

––––––––––

* Department of Physics, University of Warwick, Coventry, UK; anishur.rahman@warwick.ac.uk

[1] A. A. Penzias and R. W. Wilson, A Measurement of Excess Antenna Temperature at 4080 Mc/s., Astrophs. J. **142**, 419 (1965).

[2] D. Thornton, B. Stappers, M. Bailes, B. Barsdell, S. Bates, N. D. R. Bhat, M. Burgay, S. Burke-Spolaor, D. J. Champion, P. Coster, N. D'Amico, A. Jameson, S. Johnston, M. Keith, M. Kramer, L. Levin, S. Milia, C. Ng, A. Possenti, and W. van Straten, A population of fast radio bursts at cosmological distances, Science **341**, 53 (2013).

[3] D. Alesini, C. Braggio, G. Carugno, N. Crescini, D. D'Agostino, D. Di Gioacchino, R. Di Vora, P. Falferi, U. Gambardella, C. Gatti, G. Iannone, C. Ligi, A. Lombardi, G. Maccarrone, A. Ortolan, R. Pengo, A. Rettaroli, G. Ruoso, L. Taffarello, and S. Tocci, Search for invisible axion dark matter of mass $m_a = 43$ μeV with the quax–$a\gamma$ experiment, Phys. Rev. D **103**, 102004 (2021).

[4] A. T. M. A. Rahman, Ultrawideband axion search using a faraday haloscope, Phys. Rev. D **106**, 115017 (2022).

[5] A. Spezio, Electronic warfare systems, IEEE Trans. Microw. Theory Tech. **50**, 633 (2002).

[6] C. Li, V. M. Lubecke, O. Boric-Lubecke, and J. Lin, A review on recent advances in doppler radar sensors for noncontact healthcare monitoring, IEEE Trans. Microw. Theory Tech. **61**, 2046 (2013).

[7] L. Zhao, C. Yao, H. Wang, J. Dong, J. Zhang, X. Xu, H. Wang, B. Yao, K. Ren, L. Sun, and R. Peng, Immune

responses to multi-frequencies of 1.5 ghz and 4.3 ghz microwave exposure in rats: Transcriptomic and proteomic analysis, Int. J. Mol. Sci. **23**, 10.3390/ijms23136949 (2022).

[8] I. Goryanin, S. Karbainov, O. Shevelev, A. Tarakanov, K. Redpath, S. Vesnin, and Y. Ivanov, Passive microwave radiometry in biomedical studies, Drug Discov. Today **25**, 757 (2020).

[9] N. Thi Phuoc Van, L. Tang, V. Demir, S. F. Hasan, N. Duc Minh, and S. Mukhopadhyay, Review-microwave radar sensing systems for search and rescue purposes, Sensors **19**, 10.3390/s19132879 (2019).

[10] D. B. Chelton and F. J. Wentz, Global microwave satellite observations of sea surface temperature for numerical weather prediction and climate research, Bulletin of the American Meteorological Society **86**, 1097 (2005).

[11] D. Tse and P. Viswanath, *Fundamentals of Wireless Communication* (Cambridge University Press, Cambridge, 2005).

[12] P. Sikivie, Invisible axion search methods, Rev. Mod. Phys. **93**, 015004 (2021).

[13] C. T. Fancher, D. R. Scherer, M. C. S. John, and B. L. S. Marlow, Rydberg atom electric field sensors for communications and sensing, IEEE Transactions on Quantum Engineering **2**, 1 (2021).

[14] M. Jing, Y. Hu, J. Ma, H. Zhang, L. Zhang, L. Xiao, and S. Jia, Atomic superheterodyne receiver based on microwave-dressed rydberg spectroscopy, Nat. phys. **16**, 911 (2020).

[15] J. A. Gordon, M. T. Simons, A. H. Haddab, and C. L. Holloway, Weak electric-field detection with sub-1 Hz resolution at radio frequencies using a Rydberg atom-based mixer, AIP Adv. **9**, 045030 (2019).

[16] J. Yuan, W. Yang, M. Jing, H. Zhang, Y. Jiao, W. Li, L. Zhang, L. Xiao, and S. Jia, Quantum sensing of microwave electric fields based on rydberg atoms, Rep. Prog. Phys **86**, 106001 (2023).

[17] J. A. Gordon, M. T. Simons, A. H. Haddab, and C. L. Holloway, Weak electric-field detection with sub-1 Hz resolution at radio frequencies using a Rydberg atom-based mixer, AIP Adv. **9**, 045030 (2019).

[18] D. Budker and M. Romalis, Optical magnetometry, Nat. phys. **3**, 227 (2007).

[19] S. Graham, A. Rahman, L. Munn, R. Patel, A. Newman, C. Stephen, G. Colston, A. Nikitin, A. Edmonds, D. Twitchen, M. Markham, and G. Morley, Fiber-coupled diamond magnetometry with an unshielded sensitivity of $30\,\mathrm{pT}/\sqrt{\mathrm{hz}}$, Phys. Rev. Appl. **19**, 044042 (2023).

[20] J. Meinel, V. Vorobyov, B. Yavkin, D. Dasari, H. Sumiya, S. Onoda, J. Isoya, and J. Wrachtrup, Heterodyne sensing of microwaves with a quantum sensor, Nat. Commun. **12**, 2737 (2021).

[21] F. Couëdo, E. Recoba Pawlowski, J. Kermorvant, J. Trastoy, D. Crété, Y. Lemaître, B. Marcilhac, C. Ulysse, C. Feuillet-Palma, N. Bergeal, and J. Lesueur, High-Tc superconducting detector for highly-sensitive microwave magnetometry, Appl. Phys. Lett. **114**, 192602 (2019).

[22] G. Ranjit, M. Cunningham, K. Casey, and A. A. Geraci, Zeptonewton force sensing with nanospheres in an optical lattice, Phys. Rev. A **93**, 053801 (2016).

[23] J. Ahn, Z. Xu, J. Bang, P. Ju, X. Gao, and T. Li, Ultrasensitive torque detection with an optically levitated nanorotor, Nature nanotechnology **15**, 89 (2020).

[24] D. F. Jackson Kimball, A. O. Sushkov, and D. Budker, Precessing ferromagnetic needle magnetometer, Phys. Rev. Lett. **116**, 190801 (2016).

[25] A. T. M. A. Rahman, Large spatial schrödinger cat state using a levitated ferrimagnetic nanoparticle, New J. Phys. **21**, 113011 (2019).

[26] C. Kittel, *Introduction to solid state physics*, 8th ed. (Wiley, Hoboken, N.J, 2005).

[27] T. L. Gilbert, A phenomenological theory of damping in ferromagnetic materials, IEEE Trans. Magn. **40**, 3443 (2004).

[28] P. H. Bryant, T. L. Carroll, L. M. Pecora, and F. J. Rachford, Subsaturation ferromagnetic resonance in yttrium iron garnet spheres, Appl. Phys. Lett. **61**, 864 (1992).

[29] H. Xi, K.-Z. Gao, Y. Shi, and S. Xue, Precessional dynamics of single-domain magnetic nanoparticles driven by small ac magnetic fields, J. Phys. D: Appl. Phys. **39**, 4746 (2006).

[30] C. Mitsumata and S. Tomita, Control of gilbert damping using magnetic metamaterials, Phys. Rev. B **84**, 174421 (2011).

[31] S. I. Denisov, T. V. Lyutyy, and P. Hänggi, Magnetization of nanoparticle systems in a rotating magnetic field, Phys. Rev. Lett. **97**, 227202 (2006).

[32] H. Chang, P. Li, W. Zhang, T. Liu, A. Hoffmann, L. Deng, and M. Wu, Nanometer-thick yttrium iron garnet films with extremely low damping, IEEE Magn. Lett. **5**, 1 (2014).

[33] H. Maier-Flaig, S. Klingler, C. Dubs, O. Surzhenko, R. Gross, M. Weiler, H. Huebl, and S. T. B. Goennenwein, Temperature-dependent magnetic damping of yttrium iron garnet spheres, Phys. Rev. B **95**, 214423 (2017).

[34] F. Schreiber, J. Pflaum, Z. Frait, T. Mühge, and J. Pelzl, Gilbert damping and g factor in $Fe_x Co1_x$ alloy films, Solid State Commun. **93**, 965 (1995).

[35] E. Barati and M. Cinal, Gilbert damping in binary magnetic multilayers, Phys. Rev. B **95**, 134440 (2017).

[36] H. Keshtgar, S. Streib, A. Kamra, Y. M. Blanter, and G. E. W. Bauer, Magnetomechanical coupling and ferromagnetic resonance in magnetic nanoparticles, Phys. Rev. B **95**, 134447 (2017).

[37] P. Fadeev, C. Timberlake, T. Wang, A. Vinante, Y. B. Band, D. Budker, A. O. Sushkov, H. Ulbricht, and D. F. J. Kimball, Ferromagnetic gyroscopes for tests of fundamental physics, Quantum Sci. Technol. **6**, 024006 (2021).

[38] M. Rashid, M. Toroš, A. Setter, and H. Ulbricht, Precession motion in levitated optomechanics, Phys. Rev. Lett. **121**, 253601 (2018).

[39] A. T. M. A. Rahman, A. C. Frangeskou, P. F. Barker, and G. W. Morley, An analytical model for the detection of levitated nanoparticles in optomechanics, Rev. Sci. Instrum. **89**, 023109 (2018).

[40] R. Reimann, M. Doderer, E. Hebestreit, R. Diehl, M. Frimmer, D. Windey, F. Tebbenjohanns, and L. Novotny, Ghz rotation of an optically trapped nanoparticle in vacuum, Phys. Rev. Lett. **121**, 033602 (2018).

[41] A. T. M. A. Rahman and P. F. Barker, Optical levitation using broadband light, Optica **7**, 906 (2020).

[42] S. Kuhn, A. Kosloff, B. A. Stickler, F. Patolsky, K. Hornberger, M. Arndt, and J. Millen, Full rotational control

of levitated silicon nanorods, Optica **4**, 356 (2017).

[43] A. T. M. A. Rahman, A. C. Frangeskou, M. S. Kim, S. Bose, G. W. Morley, and P. F. Barker, Burning and graphitization of optically levitated nanodiamonds in vacuum, Sci. Rep. **6** (2016).

[44] A. T. M. A. Rahman and P. F. Barker, Measurement of the motional heating of a levitated nanoparticle by thermal light, Phys. Rev. A **107**, 013521 (2023).

[45] T. W. Penny, A. Pontin, and P. F. Barker, Sympathetic cooling and squeezing of two colevitated nanoparticles, Phys. Rev. Res. **5**, 013070 (2023).

[46] T. Delord, L. Nicolas, L. Schwab, and G. Hétet, Electron spin resonance from NV centers in diamonds levitating in an ion trap, N. J. Phys. **19**, 033031 (2017).

[47] D. S. Bykov, L. Dania, F. Goschin, and T. E. Northup, 3d sympathetic cooling and detection of levitated nanoparticles, Optica **10**, 438 (2023).

[48] Y. Jin, K. Shen, P. Ju, X. Gao, C. Zu, A. J. Grine, and T. Li, Quantum control and fast rotation of levitated diamonds in high vacuum, arXiv:2309.05821v1 (2023).

[49] S. A. Beresnev, V. G. Chernyak, and G. A. Fomyagin, Motion of a spherical particle in a rarefied gas. part 2. drag and thermal polarization, J. Fluid Mech. **219**, 405–421 (1990).

[50] M. Schuck, D. Steinert, T. Nussbaumer, and J. W. Kolar, Ultrafast rotation of magnetically levitated macroscopic steel spheres, Sci. adv. **4** (2018).

[51] J. Ahn, Z. Xu, J. Bang, Y.-H. Deng, T. M. Hoang, Q. Han, R.-M. Ma, and T. Li, Optically levitated nanodumbbell torsion balance and ghz nanomechanical rotor, Phys. Rev. Lett. **121**, 033603 (2018).

[52] S. Lee, S. Grudichak, J. Sklenar, C. C. Tsai, M. Jang, Q. Yang, H. Zhang, and J. B. Ketterson, Ferromagnetic resonance of a YIG film in the low frequency regime, J. Appl. Phys. **120**, 033905 (2016).

[53] E. G. Spencer, R. C. LeCraw, and R. C. Linares, Low-temperature ferromagnetic relaxation in yttrium iron garnet, Phys. Rev. **123**, 1937 (1961).

[54] S. Kuhn, B. A. Stickler, A. Kosloff, F. Patolsky, K. Hornberger, M. Arndt, and J. Millen, Optically driven ultrastable nanomechanical rotor, Nat. Commun. **8**, 1 (2017).

[55] A. K. Robinson, N. Prajapati, D. Senic, M. T. Simons, and C. L. Holloway, Determining the angle-of-arrival of a radio-frequency source with a Rydberg atom-based sensor, Appl. Phys. Lett. **118**, 114001 (2021).

[56] M. Huang, B. Zheng, T. Cai, X. Li, J. Liu, C. Qian, and H. Chen, Machine–learning-enabled metasurface for direction of arrival estimation, Nanophotonics **11**, 2001 (2022).

[57] Y. Arita, M. Mazilu, and K. Dholakia, Laser-induced rotation and cooling of a trapped microgyroscope in vacuum, Nat. Comm. **4**, 2374 (2013).

[58] M. F. Elmahaishi, R. S. Azis, I. Ismail, and F. D. Muhammad, A review on electromagnetic microwave absorption properties: their materials and performance, J Mater. Res. Technol. **20**, 2188 (2022).

[59] J. Van Dyck, R. S., D. L. Farnham, S. L. Zafonte, and P. B. Schwinberg, Ultrastable superconducting magnet system for a penning trap mass spectrometer, Rev. Sci. Instrum. **70**, 1665 (1999).

[60] J. W. Britton, J. G. Bohnet, B. C. Sawyer, H. Uys, M. J. Biercuk, and J. J. Bollinger, Vibration-induced field fluctuations in a superconducting magnet, Phys. Rev. A **93**, 062511 (2016).